
Continuum Models: Helping to Guide Industry

Colin Please

School of Mathematics, University of Southampton, Southampton, SO17 1BJ,
UK, cpp@maths.soton.ac.uk

Summary. This is a summary of a plenary talk given at ECMI 2008 emphasizing the importance of applied mathematics to our economies, in particular the use of continuum models to give insight and hence guide industrial developments. This is illustrated using examples from industrial study groups, where collaboration between mathematicians and industrial partners has yielded great insight.

1 Industrial Mathematics

Industrial mathematics is fundamental to the knowledge base of the economy of every country, and by its very nature it is interdisciplinary. The number of different types of applications is huge, and mathematicians have a vast array of tools to apply to help understand these problems. However, as has been discussed throughout this conference, currently it is not obvious where all these industrial mathematicians are. Andreas Schuppert suggested in his plenary talk, entitled “Mathematics in Industry – cost factor or key for profits”, that industry structures are now project-based rather than subject-based. To address this shift in strategy, industrial mathematicians must develop a wider skill base, so that they can identify appropriate mathematics for different situations, be it continuum models, statistics, operations research, computational models, etc. Since in-house research/development departments have all but disappeared, opportunities are greater for mathematicians to provide external consultancy services. One of the best ways to train and educate industrial mathematicians is to exploit the study group workshops [16]. This format has been exported all over the world, (ECMI, UK, Denmark, the Netherlands, Ireland, China and elsewhere), and has expanded to cover many different areas, (industry, plant science, medicine, geoscience). Within the study group format, mathematicians learn how to approach completely new problems, and how to collaborate with researchers from other disciplines.

2 Continuum Models in Industry

Continuum models are a rather specialised field, but they have numerous applications. However many continuum models have already been captured in computer software, and we can give many examples, e.g. “finite element analysis” of deforming solids, “CFD” of airflow over wings, heat flow in furnaces, chemical reactions in flames, and pollution dispersion in rivers. As a result, the expertise of industrial mathematicians is not so important in these areas. It is however, essential for “non-standard” problems. To identify these problems is not trivial, as we cannot expect the person with the problem to understand that mathematics would be useful. We need to be proactive and search out the opportunities.

Below we present three study group problems where continuum models have proved to be very useful. The emphasis is on simple mathematics and we shall see that even simple models are able to give good insight.

2.1 Cosmetics (Collaborators: G. Pettet, R. Colasanti, J. Malda, Z. Upton)

The manufacture of cosmetics is a multi-million dollar industry and there are countless problems that need solving. It is an interesting fact that the skin is the largest organ in the body, typically 1.5 m^2 surface area, and it is a very special sort of material. It provides many functions for the body such as protection from external sources and cooling [17]. Typical problems that the cosmetic companies are interested in include wrinkle reduction, moisturising and drug delivery (through patches or injections). They are also interested in the impact of products on the skin, such as irritation or damage caused by washing up powders.

Recent legislation has made it illegal to test detergents or cosmetics on live animals, so research is now focused on developing an artificial skin for testing. A group in Brisbane is growing artificial skin and is interacting with applied mathematicians as part of their efforts to understand how to improve their procedures. A snapshot of the skin growing in vitro is displayed in Fig. 1.

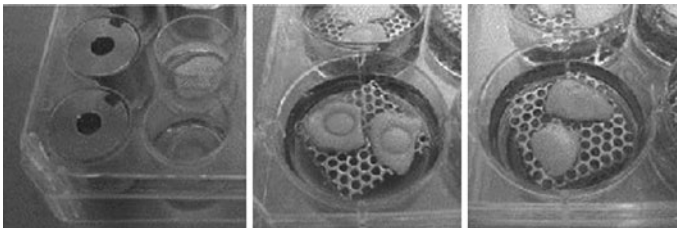


Fig. 1. Artificial skin growing in vitro. Reproduced from [1]

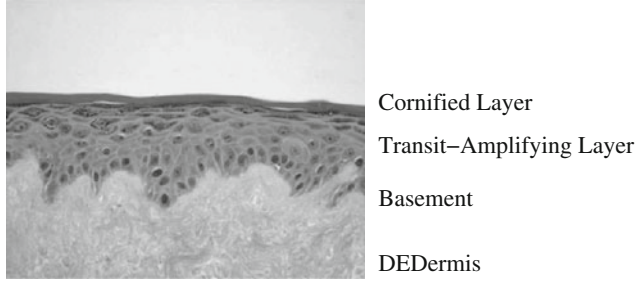


Fig. 2. Close-up photograph of artificial skin with the different layers labelled [2]

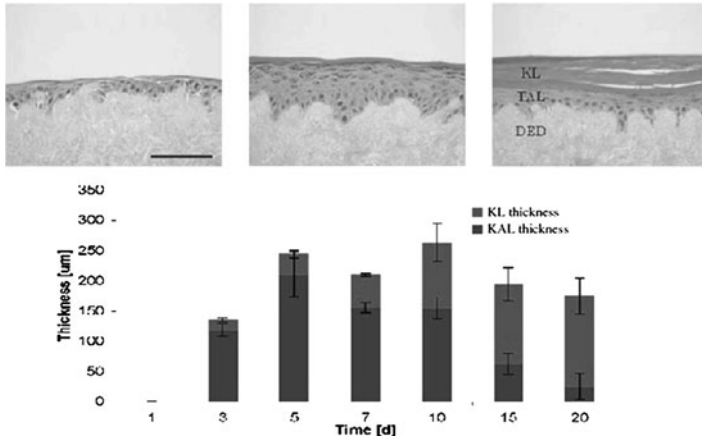


Fig. 3. Growth behaviour of human skin equivalent (HSE) [2]

Artificial skin, commonly referred to a human skin equivalent (HSE), is grown from skin taken from people. The structure of artificial skin is displayed in Fig. 2. Surplus skin is removed from the body and the top layer (the epidermis including the cornified layer (CL)) is stripped off from the dermis. The cells in the dermis are then all removed to create de-epithelised dermis (DED). A single layer of epidermal cells is then placed onto the exposed dermis and allowed to grow. The problem is to understand the resulting growth. The cells grow in the transit-amplifying layer (TAL) until they reach a certain height, where they differentiate to make the CL. In Fig. 3, we display snapshots of the different stages of growth, along with a graph showing the thicknesses of the TAL and the CL as time progresses. The first snapshot shows the TAL growing with a very thin CL on the top. As we progress to the second snapshot,

the TAL and the CL have both increased in thickness, although the CL is still much thinner than the TAL. However in the third snapshot, the TAL has thinned a lot, while the CL has thickened. The measurements displayed in the graph show how the thickness of the layers develops. This behaviour is unusual, as we would expect everything to continue thickening. The three main questions that the experiments raised were:

- Why does the TAL grow and then shrink?
- What controls the thickness of the final layers?
- Why is the interface between the TAL and the CL so flat?

To answer these questions, it is essential to understand the process of growth. Enhanced levels of nutrients cause the cells to proliferate, while high levels of calcium increase the rate of differentiation of cells from the TAL to the CL. The hypothesis suggested by the experimentalists was that the growth process depended on fluid flow. They argued that while there is no CL, fluid flow (weeping) driven by evaporation keeps calcium levels low and keeps nutrient levels high. Then as the CL recovers, the fluid flow reduces. However calculation of the Peclet number suggested that fluid flow must be irrelevant, and diffusion is more important.

An alternative theoretical approach was taken that exploited well-known observations on calcium within the epidermis. Measurements (see Fig. 4) show that there is more calcium near the CL than lower in the epidermis. It is well known that cells differentiate faster when the calcium levels are high and that differentiated cells appear to contain no calcium. Hence a model with a self-sustaining calcium gradient was developed. Calcium levels remain low initially so differentiation is slow. As the layer grows calcium at the upper surface increases in concentration as calcium is dumped into the extracellular region due to differentiation. Finally this creates the self-sustained calcium gradient.

To model the growth process the following assumptions were made:

- Cells are created/proliferate only at the lower interface between the TAL and the basement layer.
- Cells move vertically upward and are pushed from below.
- Calcium diffuses freely between cells.
- Cells take up calcium from their surroundings.
- Differentiation occurs when the concentration of calcium in the cells is sufficiently large.

We programmed these assumptions in 2D using a cellular automata program and ran simulations to visualise what happens [3]. We considered two scenarios, letting the cells start to proliferate on a flat or a bumpy layer. In both cases the cells grow upwards, the calcium concentration increases at the top and then there is a wave of retreat as the cells differentiate and throw out calcium. The process is self-sustaining.

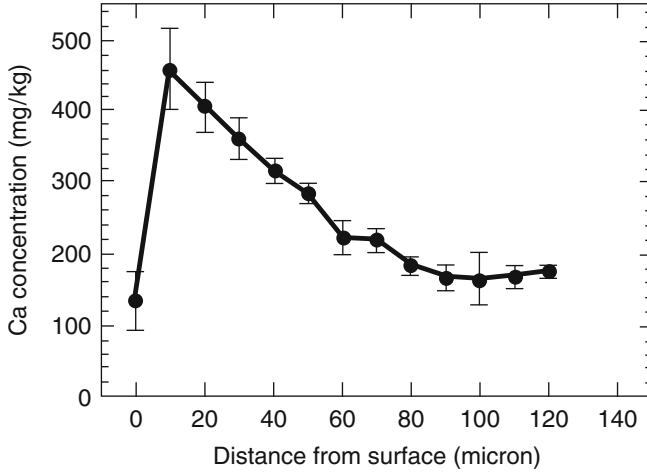


Fig. 4. Graph of calcium concentration versus distance from surface. Reproduced from [4]

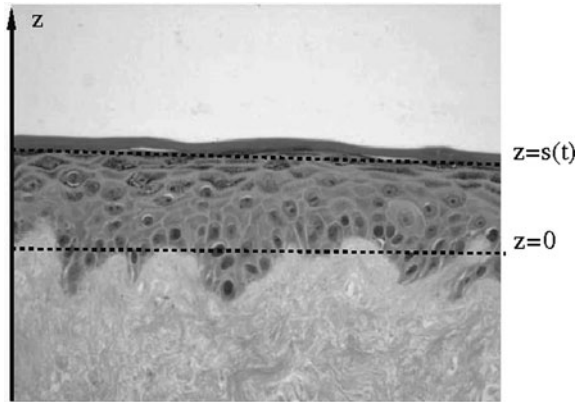


Fig. 5. A simple 1D model of the skin. The interface between the TAL and the basement layer is at $z = 0$, while the interface between the TAL and the CL is a free boundary at $z = s(t)$. Based on [2]

The cellular automata simulations produced reasonable behaviour, so we decided to write a continuum model using the same assumptions. To keep the model simple, we considered 1D, as depicted in Fig. 5. The interface between the TAL and the basement layer is at $z = 0$, while the interface between the TAL and the CL is a free boundary at $z = s(t)$. Letting $B(z, t)$ be the calcium bound in the cells and $C(z, t)$ be the freely-diffusing calcium, then the non-dimensional governing equations are

$$\left. \begin{aligned} \mu \frac{\partial^2 C}{\partial z^2} &= \mathcal{T}(C, B) \\ \frac{\partial B}{\partial t} + \frac{\partial B}{\partial z} &= \mathcal{T}(C, B) \end{aligned} \right\}, \quad 0 \leq z \leq s(t), \quad (1)$$

with boundary conditions

$$C = C_0, \quad B = B_0, \quad \text{on } z = 0, \quad (2)$$

$$\left. \begin{aligned} \frac{\partial C}{\partial z} &= \alpha B \mathcal{D}(B) \\ 1 - \frac{ds}{dt} &= \mathcal{D}(B) \end{aligned} \right\}, \quad \text{on } z = s(t), \quad (3)$$

and initial conditions

$$C = C_0, \quad B = B_0, \quad s = 0, \quad \text{at } t = 0. \quad (4)$$

Here $\mathcal{T}(C, B)$ is the transfer rate between intra-cellular and extra-cellular calcium, $\mathcal{D}(B)$ is the rate of differentiation to cornified cells, and α is a constant. To progress we chose the following forms for $\mathcal{T}(C, B)$ and $\mathcal{D}(B)$,

$$\mathcal{T}(C, B) = C - B, \quad (5)$$

$$\mathcal{D}(B) = \epsilon + \lambda H(B - 1), \quad (6)$$

where $H(\cdot)$ is the Heaviside function and λ and ϵ are constants. Equation (5) assumes that the exchange of calcium between cells is linearly dependent on concentrations. In formula (6) the ϵ term allows the cells to differentiate slowly all the time, while the Heaviside function means that when $B > 1$ the cells differentiate rapidly when the calcium level exceeds a critical value of $B = 1$. The parameter ϵ is extremely important. If ϵ is taken to be zero, then we obtain a trivial solution where the TAL simply grows and cornification never occurs. Taking $\epsilon \ll 1$ corresponds to growing a very thick TAL before $B = 1$ and cornification occurs. Therefore ϵ is the trigger mechanism which switches on the calcium gradient.

Examples of the behaviour of the model are shown in Figs.6 and 7. In both cases the model reproduces the gradient of the calcium concentration, which increases towards the top of the TAL ($z = s(t)$). The graphs of layer thickness versus time show that $s(t)$ increases and then decreases, replicating the observed growth and retreat of the TAL. The model also reproduces the thickening in the CL which is shown between the curves of $s(t)$ and the outer surface $\eta(t)$. Depending on the values chosen for ϵ and λ , the thickness of the TAL may oscillate over time, as can be seen in Fig.7. This oscillatory behaviour has yet to be seen experimentally.

To summarize, the continuum model fits the observed experimental data, although there is some data fitting due to lack of experimental evidence for

the different parameters. Future work includes extending the model to 2D or 3D to see if the free boundary between the TAL and the CL remains flat. We also need to consider more details of the flow of cells in the TAL, and we should incorporate other mechanisms to understand the trigger (cell death, potassium etc.).

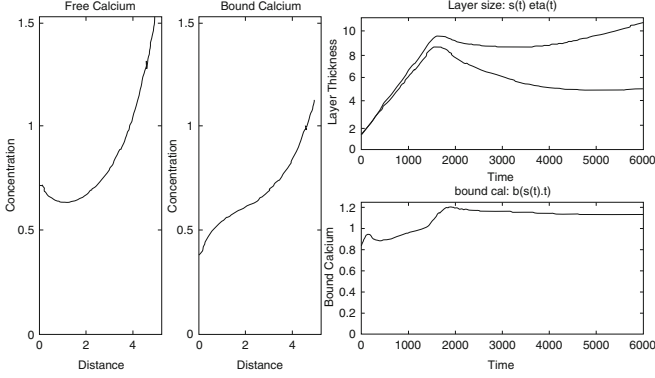


Fig. 6. Typical conditions. The graphs of free and bound calcium versus z are snapshots at time $t = 6,000$, where the interface $s(t) \approx 4.8$. The graph of layer thickness versus time shows the top of the TAL ($s(t)$, *lower line*) and the CL ($\eta(t)$, *upper line*)

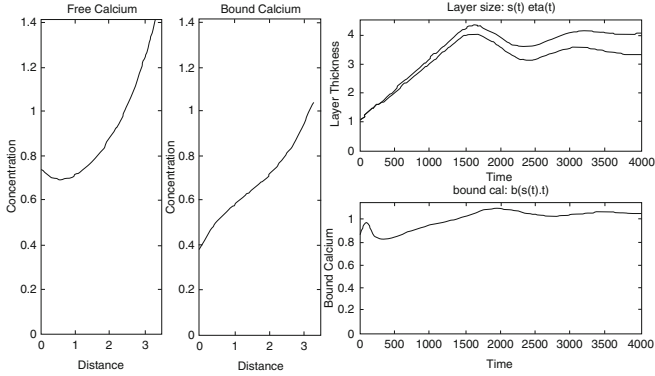


Fig. 7. Differentiation has high sensitivity to calcium. The graphs of free and bound calcium versus z are snapshots at time $t = 4,000$, where the interface $s(t) \approx 3.3$. The graph of layer thickness versus time shows the top of the TAL ($s(t)$, *lower line*) and the top of the CL ($\eta(t)$, *upper line*)

2.2 Optical Fibres (Collaborators: D. Abbott, P. Howell, A. Fitt, C. Voyce, B. Tilley, D. Schwendeman, T. Monro and Others)

The second problem that we shall consider concerns optical fibres. Optical fibres are used extensively in communications systems or optical detectors. These fibres have spawned many areas of research including investigation of their electromagnetic and mechanical properties. In this section we are interested in the actual manufacturing process. This problem was brought to a study group by Corning Inc [5].

Optical fibres work by using changes in the refractive index to guide light down the glass core of the fibre. Usually the glass is doped to provide the change in refractive index, but an alternative is to make the fibre with an array of holes down the centre, with cross-sections such as those as displayed in Fig. 8. The transition from the air to the glass provides the required changes in refractive index. One way to make the holey fibre is to take hollow straws of glass ≈ 1 m long and pack them together into a bundle of diameter ≈ 3 cm, with a solid straw in the middle, thereby creating a ‘blank’. The blank is put in a furnace and drawn out into a fibre ≈ 100 km long with diameter measured in μm . The aspect ratio of the blank therefore changes by order 10^5 . Corning are interested in what happens to the fibre in the drawing process, especially as surface tension will try to close the holes off. They are also interested in the behaviour of any bubbles within fibres, as these will cause problems. The evolution of bubbles and holes may be described by identical equations. There are a number of papers that study this problem including [7, 8] and [9] and the work here follows these ideas closely. The precise problem is discussed in more detail in the presentations available at [5].

To gain a basic understanding of the behaviour we take a simple case and consider the behaviour of one hollow straw of glass. We assume that the straw

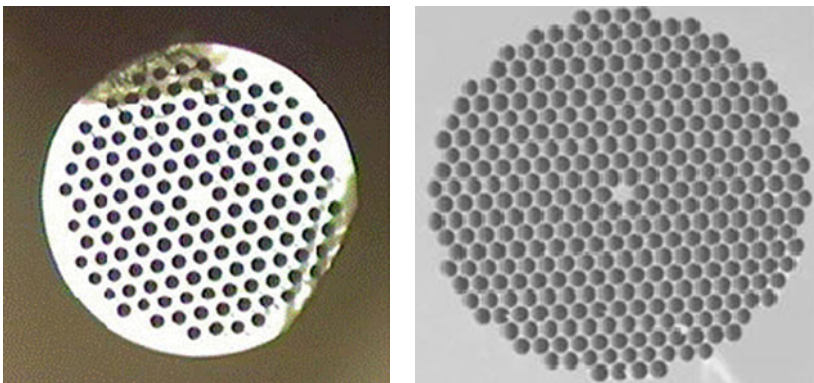


Fig. 8. Example cross-sections of ‘holey’ optical fibres [6]

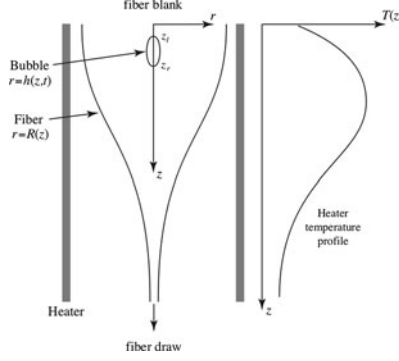


Fig. 9. Schematic of a fibre with a single concentric bubble or hole. Reproduced from [5]

is axis-symmetric and that the glass is a Newtonian viscous fluid. A schematic of the model is shown in Fig. 9. The radius of the hole is given by $r = h_1(z, t)$, where z is the vertical coordinate measured from the exit of the furnace. The radius of the glass is given by $r = h_2(z, t)$. Taking advantage of the long thin aspect ratio to neglect appropriate terms, the governing equations for the evolution of the fibre in the z -direction are

$$\rho(h_2^2 - h_1^2) \left(\frac{\partial w}{\partial t} + w \frac{\partial w}{\partial z} + g \right) = \frac{\partial}{\partial z} \left(3\mu(h_2^2 - h_1^2) \frac{\partial w}{\partial z} + \gamma(h_1 + h_2) \right), \quad (7)$$

$$\frac{\partial(h_2^2 - h_1^2)}{\partial t} + \frac{\partial(w(h_2^2 - h_1^2))}{\partial z} = 0, \quad (8)$$

$$\frac{\partial h_1^2}{\partial t} + \frac{\partial w h_1^2}{\partial z} = \frac{p h_1^2 h_2^2 - \gamma h_1 h_2 (h_1 + h_2)}{\mu(h_2^2 - h_1^2)}. \quad (9)$$

Here ρ and μ are the density and viscosity of the glass and γ is the surface tension of the glass in air. Gravity is represented, as usual, by g . The vertical velocity of the glass is denoted by $w(z, t)$ and $p(z, t)$ represents the pressure, above atmospheric, of gas in the hole. Boundary conditions are prescribed on the free surfaces $r = h_1(z, t)$ and $r = h_2(z, t)$, and also at the top $z = 0$ and the bottom $z = L$. Equation (7) represents conservation of momentum in the z -direction, (8) represents conservation of mass, and (9) represents conservation of momentum in the radial direction. The coefficient of $\partial w / \partial z$ in the first equation is known as the Trouton viscosity.

Suppose that we now consider the small hole limit, so that $h_1(z, t) \ll h_2(z, t)$. Then to leading order (7)–(9) reduce to

$$\rho h_2^2 \left(\frac{\partial w}{\partial t} + w \frac{\partial w}{\partial z} + g \right) = \frac{\partial}{\partial z} \left(3\mu h_2^2 \frac{\partial w}{\partial z} + \gamma h_2 \right), \quad (10)$$

$$\frac{\partial(h_2^2)}{\partial t} + \frac{\partial(wh_2^2)}{\partial z} = 0, \quad (11)$$

$$\frac{\partial h_1^2}{\partial t} + \frac{\partial(wh_1^2)}{\partial z} = ph_1^2 - \gamma h_1. \quad (12)$$

Note that in this case the last equation for the radius of the hole has decoupled. This means that as we draw the blank, the glass acts as if there were no hole and the hole is forced to change in response to the glass flow. We may rewrite the last equation as

$$\frac{\partial a}{\partial t} + \frac{\partial(wa)}{\partial z} = pa - \gamma\sqrt{a}, \quad (13)$$

where $a(z, t)$ is the cross-sectional area of the hole. The evolution of a depends on the competition between the pressure p in the hole, which tries to keep the hole open, and the surface tension γ , which tries to close the hole. Corning want to keep the hole open, and tried changing the pressure in the hole to achieve this. However this was not very successful, and this may be explained by considering (13). This is a hyperbolic equation for a , and we can see that if the term pa dominates, then a will grow exponentially, while if $\gamma\sqrt{a}$ dominates, then the hole will pinch off. It is therefore extremely difficult to use the pressure to control the difference in these two terms and make the hole stay at the unstable equilibrium point $a = (\gamma/p)^2$.

Equation (13) also enables us to analyse how the shape and size of a bubble changes as a fibre is drawn. Suppose that at $t = 0$, the top and bottom of the bubble lie at z_{\min} and z_{\max} respectively. Then the bounding characteristics generated by (13) will tell us within what range the bubble lies. The bounding characteristics will have a profile similar to that depicted in Fig. 10, so that the bubble elongates as drawing progresses, (as long as pinch-off does not occur).

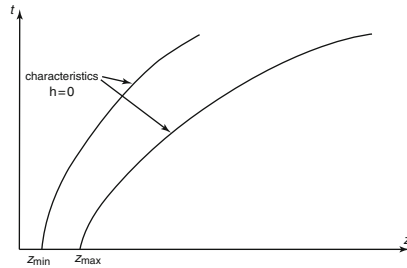


Fig. 10. Typical bounding characteristics which determine bubble evolution during the drawing process. Reproduced from [5]

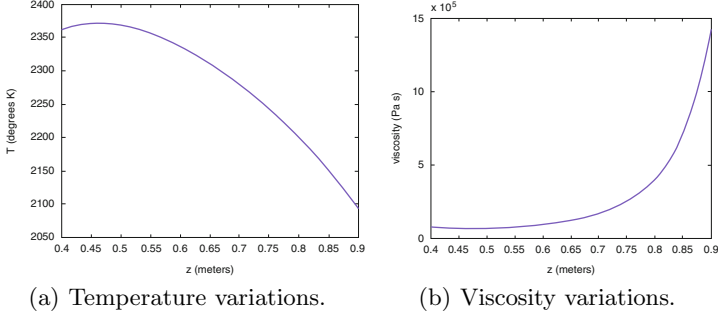


Fig. 11. Typical temperature and viscosity variations in the z -direction as the fibre is drawn. Reproduced from [5]

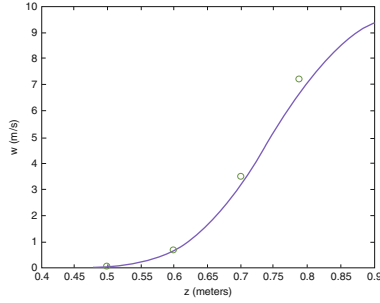


Fig. 12. Vertical velocity of the glass in the steady state, $w(z)$. Reproduced from [5]

To allow us to solve (10)–(12) we may reasonably assume that the density and surface tension of the glass are constant. However it is not so clear that we can assume a constant viscosity as the temperature variations down the fibre are large. We show typical temperature and viscosity variations in Fig. 11. Perhaps surprisingly the variations in viscosity are not extreme and as an approximation we may take it to be constant at around 10^6 Pa s. Imposing appropriate boundary conditions and assuming a steady glass flow, we solved (10) and (11) numerically for the velocity w , and the results are shown in Fig. 12.

Using this solution for $w(z)$, we may solve (12) for the evolution of a bubble. In doing this we will assume that the pressure in the bubble is spatially uniform, this assumes the gas can move easily inside it, that the mass of gas is constant and that the gas is governed by the ideal gas law. In this way the pressure varies both due to the changes in bubble shape and due to temperature variations along the fibre. The numerical solution for the evolution of

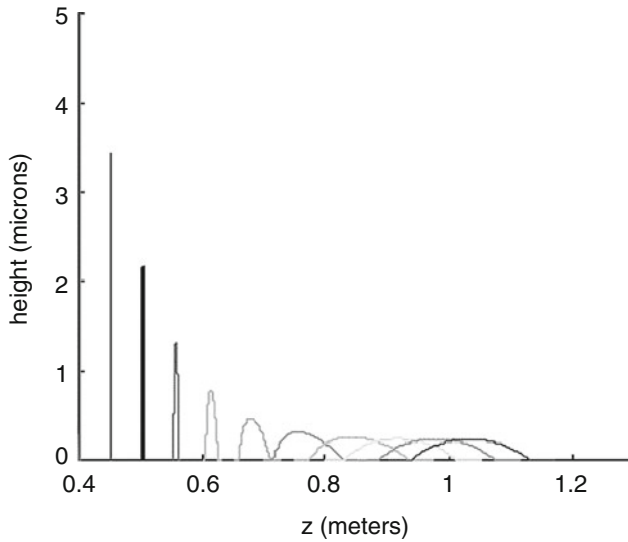


Fig. 13. Numerical solution for the steady state evolution of a bubble down the fibre. Reproduced from [5]

a bubble is shown in Fig. 13. The sharp peak at $z \approx 0.4$ represents a bubble near the top of the fibre with maximum radius $5\mu\text{m}$, with the top and bottom of the bubble very close together ($5\mu\text{m}$). The subsequent shapes represent the evolution of the bubble as it progresses down the fibre, and we can see that it elongates dramatically and the radius decreases. For example, the peak at $z \approx 1\text{m}$ shows that the maximum radius of the bubble has decreased to approximately $0.25\mu\text{m}$, while the distance between the top and bottom of the bubble has increased to approximately 0.2m . Corning calls these elongated bubbles threads, and would like to eliminate them.

The pressure within the bubble is shown in Fig. 14 and indicates that it increases in the hot region and then decreases in the solidifying region. Note also that, although the bubbles are elongated by the stretching of the glass they can be shown to be shorter than the length that would be predicted by the simple argument about bounding characteristics because the ends pinch-off.

Although many assumptions have been made, the continuum model proposed above has been able to provide great insight into the control of holes and the size of bubbles. A further item of interest would be to consider the effect of gas leaving the bubble by diffusion into the surrounding glass, which would affect the pressure. In addition, realistic fibres enclose thousands of bubbles,

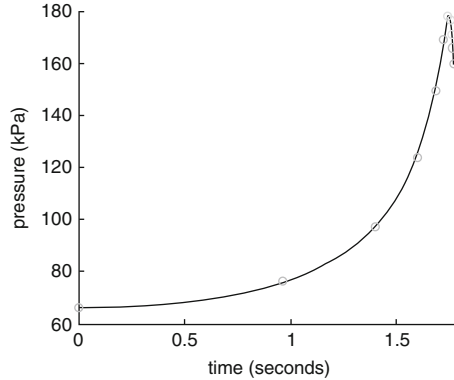


Fig. 14. Pressure in the bubble versus time (*circles* correspond to the times of the *bubble shapes* in Fig. 13). Reproduced from [5]

not just one, so it would be interesting to apply homogenisation techniques to extend the analysis for the single bubble.

2.3 Semiconductors (D. Schwendeman, P. Kramer, T. Witelski, L. Borucki)

Years ago the field of semiconductor modelling was perfect for the use of asymptotic analysis, as the important non-dimensional parameter, the ratio of the Debye length to the device size, was $O(10^{-10})$. However as technology has advanced and the size of the devices has decreased, this number is now approximately 10^{-1} or larger, and as a result the original asymptotic results are less applicable! There are two main aspects to semiconductor modelling:

1. Manufacturing processes
 - Etching
 - Lithography
 - Deposition
 - Implantation
2. Electrical behaviour
 - Quantum effects
 - Solar cell efficiency

In particular, there are many opportunities for the use of mathematics in modelling the quantum effects. Currently the engineers include these effects in a very much empirical manner (for some interesting quantum analysis see [10]).

In this section we concentrate on manufacturing aspects of the devices. The semiconductors are constructed from multiple layers, which are added

in separate processes (deposition, lithography, etching). It is very important to have a flat surface for each lithographic stage. As the multiple layers are added, each layer becomes more bumpy, and this affects the focusing required for accurate lithography. To avoid this difficulty, the surface is frequently polished flat using Chemical Mechanical Polishing. This process is not only abrasive, but also uses dissolving chemicals.

The Chemical Mechanical Polishing process uses three spinning discs. A cartoon of the polisher is shown in Fig. 15. The semiconductor wafer to be polished is stuck onto the bottom of the wafer carrier, which spins the wafer round and presses it onto the polishing pad. The polishing pad revolves in the opposite direction at the same angular speed (by having the same angular speed the relative velocity of the wafer and the polishing pad is independent of position so polishing will be quite uniform). A cross-section of this pad, as shown in Fig. 16, is abrasive and provides the mechanical element of the polishing while its surface is sprayed with a slurry to provide the chemical element of the polishing. There is a third spinning disc, which is the conditioning disc. As the polishing pad spins round it wears down and the conditioner renews the surface.

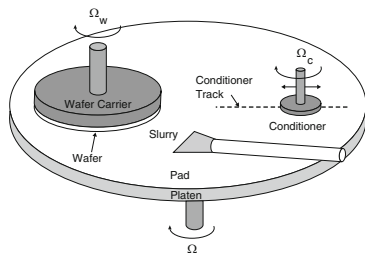


Fig. 15. Cartoon of Chemical Mechanical Polisher. Reproduced from [11]

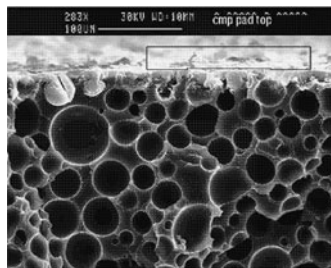


Fig. 16. Cross-section through a polishing pad. Reproduced from [11]

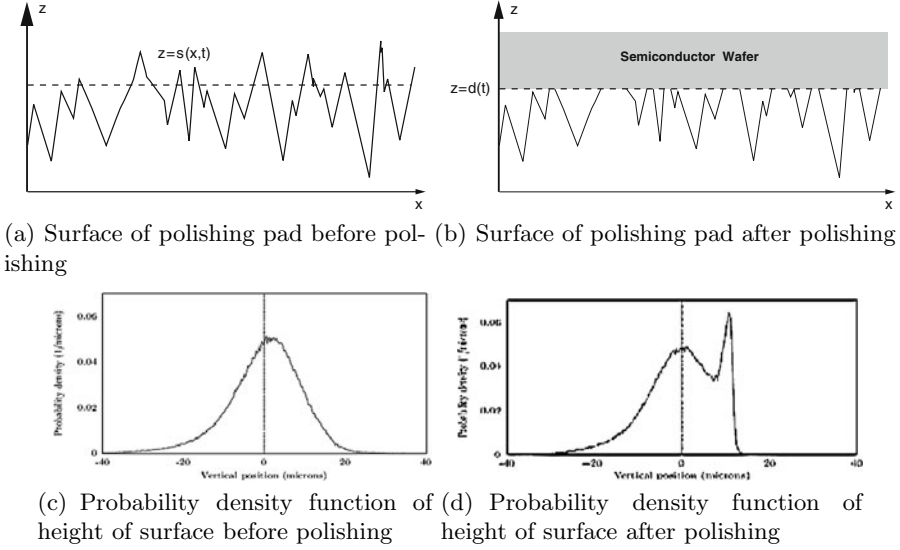


Fig. 17. Model of the surface of the polishing pad. Reproduced from [11]

The problem posed by Motorola at the study group was to investigate how the rough surface of the polishing pad changes as it is subjected to both wear and to conditioning. We were able to pose this as a continuum problem and a more detailed description much of the following is given in [11] and the study group report [12].

Let us first of all consider the wearing of the polishing pad. Before polishing, the surface of the pad will have a jagged surface, which we may represent by the function $z = s(x, t)$ as displayed in Fig. 17(a). If we let $\phi(z, t)$ be the probability density function of the height $s(x, t)$, then a graph of $\phi(z, t)$ will have a profile of the form depicted in Fig. 17(c). When the pad is used to polish the semiconductor wafer, because the wafer is hard and the pad quite compliant, the jagged surface will be flattened at a certain height $z = d(t)$, as shown in Fig. 17(b) and the flatten regions will then wear. Because of the wear the amount of pad surface at height $z = d(t)$ will increase and a spike develops in the probability density function at this height, as we can see in Fig. 17(d). This general behaviour will now be described mathematically.

The displacement of any point on the pad surface by the semiconductor wafer pressing down on it is given by $(z - d(t))H(z - d(t))$, where $H(\cdot)$ is the Heaviside function. If we assume that the wear-rate of the surface is proportional to the square root of the displacement (Hertzian indenter), then by conservation of probability, we may write down

$$\frac{\partial \phi}{\partial t} + \frac{\partial}{\partial z} \left(\beta \sqrt{(z - d(t)) H(z - d(t))} \phi \right) = 0, \quad (14)$$

where β is the constant of proportionality.

Letting $q(z, t)$ be the fraction of solid pad in any plane $z = \text{constant}$, then $q(z, t) = \text{Prob}(z < s(x, t))$, which is the cumulative density function. We therefore have the following relationship between q and ϕ :

$$\phi(z, t) = -\frac{\partial q(z, t)}{\partial z}, \quad (15)$$

and (14) may be rewritten, after using conditions when $z \rightarrow -\infty$, as

$$\frac{\partial q}{\partial t} + \beta \sqrt{(z - d(t)) H(z - d(t))} \frac{\partial q}{\partial z} = 0. \quad (16)$$

Now let us consider the conditioning process. The conditioner consists of a circular plate on which a regular array of small sharp diamonds are adhered. As the conditioner is pressed against the polishing pad the diamonds cut grooves into the surface of the polishing pad. The cuttings from the pad are removed in the slurry and the interwoven grooves create the new surface of the polishing pad. As a simple model we shall assume that we need consider only one diamond and that this moves randomly cutting grooves in a prescribed spatial interval. A cartoon of this process is shown in Fig. 18. Where the diamond is represented by the thin shaded triangle, and its endpoint is assumed to be at a height $z = h(t)$. The pad has a groove cut in it in the region $z - h(t) > 0$, and if the cutter has straight sides, it may be shown that

$$\frac{\partial q}{\partial t} = -\gamma(z - h(t))H(z - h(t))q, \quad (17)$$

where $q(z, t)$ is the cumulative density function mentioned above and γ is a constant of proportionality which measures the sharpness, or more specifically the steepness of the sides, of the cutter. Putting (16) and (17) together, for simultaneous wearing and conditioning, $q(z, t)$ satisfies the equation

$$\frac{\partial q}{\partial t} = \beta \sqrt{(z - d(t)) H(z - d(t))} \frac{\partial q}{\partial z} - \gamma(z - h(t))H(z - h(t))q, \quad (18)$$

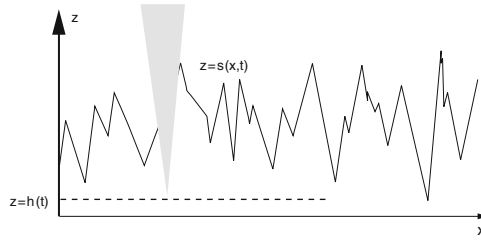


Fig. 18. Conditioning process using a *diamond* (represented by the *shaded triangle*) to cut a groove in the polishing pad below

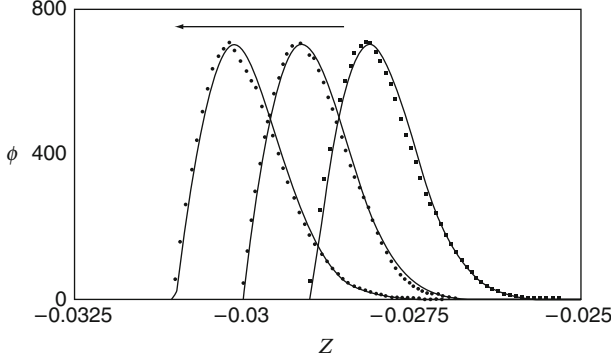


Fig. 19. Probability density function for wear of the polishing pad. The model results are represented by the *continuous line*, and the experimental results by *dots*. Reproduced from [11]

which is a linear hyperbolic partial differential equation. Usually the conditioning plate and the wafer are pressed down at a given rate, c , so we consider a “steady” problem where

$$h(t) = h_0 - ct, \quad d(t) = D + h(t) = D + h_0 - ct. \quad (19)$$

Looking for a travelling wave solution, $q(\eta)$, where η is a moving variable defined by $\eta = z - h(t)$, (18) reduces to a linear ordinary differential equation:

$$c \frac{\partial q}{\partial \eta} = \beta \sqrt{(\eta - D) H(\eta - D)} \frac{\partial q}{\partial \eta} - \gamma \eta H(\eta) q. \quad (20)$$

Solving (20), with appropriate conditions at infinity, in the case when no conditioning is applied and $\gamma = 0$ allows us to determine a probability density function ϕ as shown in Fig. 19. Solving (20) to include both the wear and the conditioning of the pad produces a probability density function as shown in Fig. 20. In both graphs the experimental results are marked with dots, and the model gives an excellent fit.

To conclude, the continuum model gives an excellent fit to the experimental data with very little parameter fitting. There are of course improvements that can be made to the model. We currently assume that the material of the polishing pad is solid. In fact it actually contains many cavities, as can be seen in Fig. 16. The initial data is not a delta function, representing a flat surface, but has a distribution, representing the cavities in the pad, and each new cut of the conditioner now exposes material with this distribution rather than cutting solid material.

2.4 Wine Making

The last problem is to do with wine making, and, rather than demonstrating the effectiveness of continuum modelling, it serves as cautionary tale to

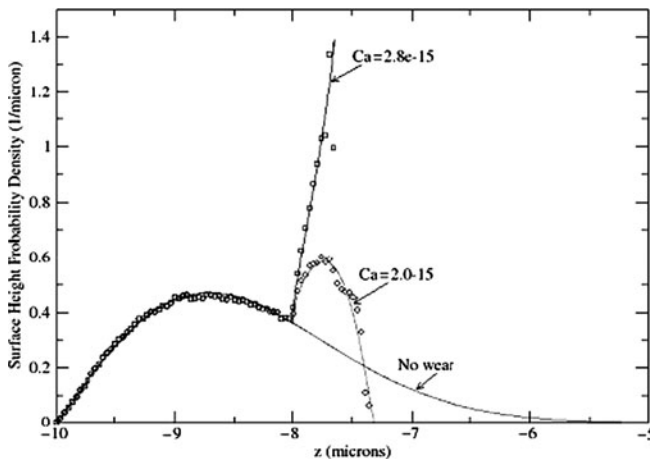


Fig. 20. Probability density function for simultaneous wear and conditioning of the polishing pad. The model results are represented by the *continuous line*, and the experimental results by *dots*. Reproduced from [11]

modellers working with industry. There are many problems in the wine making industry, for example how to spray the grapes to ensure total coverage [13], but one particular problem was brought by an Australian company that had problems with the labels starting to peel off their bottles [14, 15]. The modellers at the study group duly went away and considered many interesting problems, such as bubbles under the labels, the dynamics of the labelling machine and the modelling of the glue on the paper. However, it was only when someone did a simple experiment of actually trying to put a label onto a bottle that the answer became apparent. Paper is not orthotropic and tries to curve in one direction. To label bottles securely, the curvature of the label must be at right angles to the curvature of the bottle. Then the curvatures counteract each other and the label stays on. This fact has been well-known for years, was assumed to have been accounted for, but has somehow been overlooked in the quality assurance process. So the warning to modellers is that, before leaping ahead with all sorts of complicated mathematics, ensure that you have understood some of the basics first.

3 Overview

This article has reviewed several areas where continuum mathematics can be applied to solve industrial problems. For many physical problems some continuum models are relatively accessible to non-mathematicians as they are already coded into usable software. To be effective industrial mathematicians must therefore interact strongly with the industrialists to identify

“non-standard” problems because these provide opportunities for mathematics to have a significant impact in understanding the problem. In seeking these new problems it is important to note that although it is very motivating to involve complicated mathematics, the complexity of the mathematics may not always be correlated to the insight that it gives. The examples quoted show that simple mathematics, suitably applied, can produce understanding that allows problems to be solved. Finally the scope of continuum mathematics is vast and hence it can guide industrialists in an extremely wide range of areas.

Acknowledgements

Many thanks to Chris Bell for his assistance in the creation of this manuscript.

References

1. Topping, G., Malda, J., Dawson, R.A., Upton, Z.: *Prim. Intention*. **14**, 14–21 (2006)
2. Malda, J.: personal communication.
3. <http://ric.colasanti.googlepages.com/camodels2>
4. Mauro, T., Bench, G., Siddaras-Haddad, E., Feingold, K., Elias, P., Cullander, C.: *J. Invest. Dermatol.* **111**(6), 1198–1201 (1998)
5. <http://www.math.wpi.edu/MPI2008/corning/corningMPI2008.pdf>
6. Monroe, T.M.: personal communication.
7. Fitt, A.D., Furusawa, K., Monro, T.M., Please, C.P., Richardson, D.J.: *J. Eng. Math.* **43**, 201–227 (2002)
8. Voyce, C.J., Fitt, A.D., Monro, T.M.: *Opt. Express*. **12**, 5810–5820 (2004)
9. Voyce, C.J., Fitt, A.D., Monro, T.M.: *J. Lightwave Technol.* **26**(7), 791–798 (2008)
10. Cumberbatch, E., Uno, S., Abebe, H.: *Euro. J. Appl. Math.* **17**, 465–489 (2006)
11. Borucki, L.J., Witelski, T., Please, C.P., Kramer, P.R., Schwendeman, D.W.: *J. Eng. Math.* **50**, 1–24 (2004)
12. <http://www.wpi.edu/Academics/Depts/Math/News/MPI2005/FinalReports/Araca.pdf>
13. Barry, S.I., Weber, R.O.: In Hewitt J. (ed.) *Proceedings of the 2001 Mathematics-in-Industry Study Group*, pp. 28–40. ISBN 0-9578623-1-8, MISG. (2001)
14. Broadbridge, P., Fulford, G.R., Fowkes, N.D., Chan, D.Y.C., Lassig, C.: *SIAM Rev.* **41**(2), 363–372 (1999)
15. Hewitt, J. (ed.): *Proceedings of the 1996 Mathematics-in-Industry Study Group*, pp. 103–113. ISBN 0-646-28979-9, MISG. (1996)
16. <http://miis.maths.ox.ac.uk/>
17. http://www.infovisual.info/03/036_en.html

Progress in Industrial Mathematics at ECMI 2008

Fitt, A.D.; Norbury, J.; Ockendon, H.; Wilson, E. (Eds.)

2010, XXI, 1083 p., Hardcover

ISBN: 978-3-642-12109-8